GA–A24110

STEERABLE, MILLIMETER WAVE, SPARSE ARRAY FOR SATELLITE OBSERVATIONS UNDER CLOUDY CONDITIONS ON HALEAKALA

by
R.T. SNIDER and T.L. RHODES

DATE PUBLISHED: SEPTEMBER 2002

GA–A24110

STEERABLE, MILLIMETER WAVE, SPARSE ARRAY FOR SATELLITE OBSERVATIONS UNDER CLOUDY CONDITIONS ON HALEAKALA

by
R.T. SNIDER and T.L. RHODES*

This is a preprint of a paper to be presented at the 2002 AMOS Technical Conference, Maui, Hawaii, September 13–14, 2002 to be published in the Proceedings.

Work supported in part
under U.S. Department of Energy
Grant DE-FG03-01ER54615

*University of California at Los Angeles, Los Angeles, CA

GENERAL ATOMICS PROJECT 04437
DATE PUBLISHED: SEPTEMBER 2002

STEERABLE, MILLIMETER WAVE, SPARSE ARRAY FOR SATELLITE OBSERVATIONS UNDER CLOUDY CONDITIONS ON HALEAKALA

R.T. Snider
General Atomics, Photonics Division, 10240 Flanders Court, San Diego, California 92121-2901
T.L. Rhodes
University of California at Los Angeles, Los Angeles, California

ABSTRACT

The Air Force Maui Optical and Supercomputing (AMOS) facility is a contributing sensor to the Space Surveillance Network (SSN). It is tasked by Air Force Space Command (AFSPC) to provide metrics and space object identification and operates continuously (24/7). Weather is the primary hindrance to AMOS operation. Over the last 10 years, statistics show an approximate 30% outage primarily caused by weather. One of the major contributors to weather outages is clouds. Several spectral bands in the millimeter wave (MMW) region exist with significantly lower water absorption than visible or infrared radiation. Because of the low water absorption, thermal radiation in these MMW bands, either reflected or emitted from objects in low earth orbit, can be imaged on the ground through thick clouds. In this paper we will describe a concept for a MMW imaging system compatible with the AMOS Haleakala site that can image and track objects in low earth orbit through heavy clouds.

At the long wavelengths considered a 300 to 600 meter aperture would be required for resolving a one-meter satellite in low earth orbit. A conventional mirror or lens of this size would be impractical and a conventional sparse pupil array would require an unwieldy many tens of thousands of elements in order to achieve the required spatial resolution and coverage of the sky. However, a sparse array made up of several hundred elements with individually steerable antennas could provide the resolution, signal to noise and sky coverage required by the AMOS facility.

Basic elements and issues associated with the array including the MMW receivers, electronically steerable mirrors, motion compensation, image reconstruction algorithms and array design optimization will be discussed.

1. INTRODUCTION

The AMOS role in the SSN, to provide metrics and space object identification on a continuous basis, is primarily fulfilled by visible or infrared imaging systems [1]. While these systems provide outstanding image quality and clarity they are hindered by cloud cover. Due to the local weather patterns at the AMOS Haleakala site cloud coverage contributes significantly to AMOS down time. While there are several possible techniques for reducing or eliminating the impact of clouds on the AMOS mission, including high power laser illumination [2], and long wavelength radar systems, we discuss here the role a passive MMW imaging sensor might play in the overall AMOS mission. MMW radiation, roughly 60 GHz (5 mm) to 300 GHz (1 mm), is of potential interest for several reasons: (1) atmospheric absorption is in general less then in the visible and infrared (IR) regions, and there exist spectral bands in the MMW regions with very low water and oxygen absorption; (2) existing MMW detectors have enough sensitivity to detect thermal emission from room temperature bodies; (3) the wavelengths are short enough that acceptable spatial resolution at the space object is possible with a reasonable sized real aperture on the ground.

2. ATMOSPHERIC ABSORPTION

Absorption of MMW radiation through the atmosphere is dominated by absorption by O_2 and water. Water vapor has spectral absorption lines at roughly 22 GHz, 183 GHz and 325 GHz while oxygen has absorption lines near 60 GHz and 118 GHz as shown in Fig. 1 [3]. Water absorption in the spectral regions between these absorption lines dominates for all but the driest of conditions. (In the region around 95 GHz absorption from other atmospheric constituents play an important role when the relative humidity is less then ~15%.) Based on Fig. 1., there are three regions of interest with low atmospheric absorption, 94 GHz, 140 GHz and 220 GHz. Table 1. lists the atmospheric absorption for these three bands under various weather conditions.

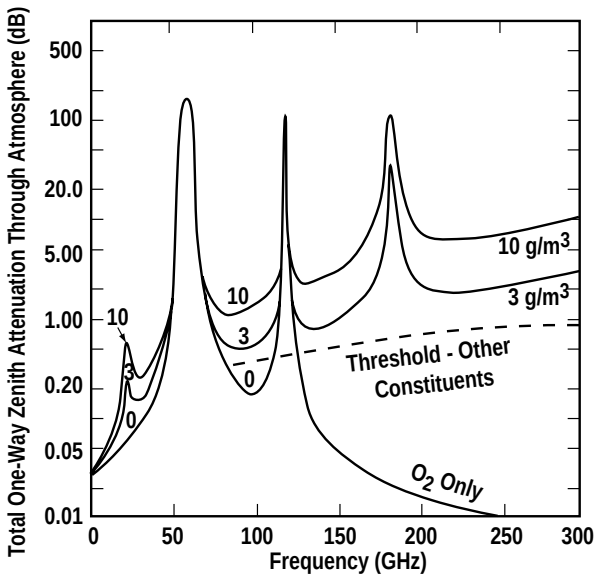

Fig. 1. Total one-way zenith attenuation from the JPL radiative-transfer program for 0, 3, and 10 g/m^3 water (2-km scale height) (U.S. Standard Atmosphere, 1976). Surface temperature 2800 K; 1 to 300 GHz.

Table 1. MMW Atmospheric Losses vs Weather. View is at Zenith

Weather Conditions	98 GHz L_{atm} (dB/km)	140 GHZ L_{atm} (dB/km)	220 GHZ L_{atm} (dB/km)
Clear (7.5 g/m^3, 50% relative humidity)	0.4	1.2	3.5
Clear (12 g/m^3 100% relative humidity)	0.8	1.5	4.0
Overcast, cloud (0.5 km thick)	1.2	2.0	5.0
Light rain (<4 mm/h)	1.6	2.4	5.5

While the thermal emission from room temperature objects peaks in the IR there is still sufficient thermal radiation to obtain passive images with good signal-to-noise ratio (SNR) using existing detectors in the MMW region. Coupled with the lower attenuation of MMW radiation through weather there is an advantage in using a MMW imaging system for thermal imaging through clouds as shown in Fig. 2.

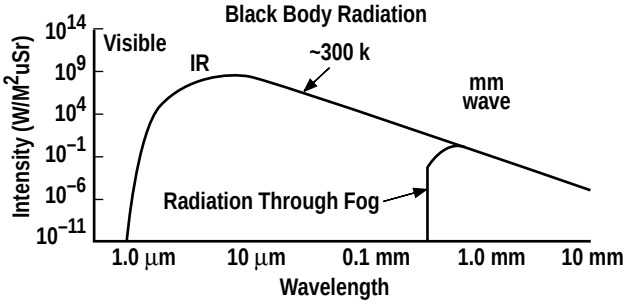

Fig. 2. Intensity of radiation as a function of wavelength from a room temperature block body through clear air and fog.

3. SPATIAL RESOLUTION/ANTENNA SIZE

In the best case the MMW imaging system spatial resolution would be limited by diffraction. For a circular aperture the spatial resolution limit (r) is given approximately by Eq. (2) r =1.3 λ *R/D* where *R* is the range to the object, and *D* is the diameter of the imaging aperture. The choice of wavelength within the MMW region is driven by the spatial

resolution, weather penetration (Fig. 1) and by available receivers where both cost and performance are an issue. While the resolution requirements (which drive the aperture size) favor the shorter wavelength bands at 140 GHz and 220 GHz, the atmospheric absorption is greater at the shorter wavelengths and the detectors are considerably more expensive and somewhat noisier. With the current state of the receiver technology and the spatial resolution requirements, 94 GHz is probably the best near term choice. For spatial resolution at the space object of 2 m, a wavelength of 3 mm (94 GHz) and a range of 200 km the aperture size for the imaging system is about 300 m. Existing linear (Two-MU [4]) and nonlinear (Maximum Likelihood and Maximum a-Priori [4,5] for example) algorithms show promise in allowing extraction of features in passive MMW images as small as half the diffraction limit. This would allow finer resolution, around 1 m, at 200 km range.

A MMW radiometer on the ground observing a space object would receive radiation contributions from various sources as shown in Fig. 3. The effective temperature seen by a receiver on the ground from the solid angle subtended by the space object is given approximately by

$$T_{\text{received}} = T_{\text{reflected earth}} + T_{\text{atmos}} + T_{\text{object}} \tag{1}$$

and the effective temperature of the surrounding background (space) is given approximately by

$$T_{\text{background}} = T_{\text{space}} + T_{\text{atmos}} \tag{2}$$

where we have assumed that most of the radiation received is in the main lobe of the imaging antenna pattern. (This will be discussed in more detail later.) The terms on the right in Eqs (1) and (2) are the effective temperatures of the sources as seen by the receiver on the ground. The MMW radiation passing through the atmosphere is attenuated reducing the effective temperature as seen by the ground receiver. The effective temperature of the contributing sources in Eqs (1) and (2) are related to the physical temperatures by: $T_{\text{reflected earth}} = (1-\varepsilon)\, T_{\text{earth}}/L_a$; $T_{\text{atmos}} = T_a\,(1 - 1/L_a)$; $T_{\text{object}} = \varepsilon T_o/L_a$; and $T_{\text{space}} = T_s/L_a$ where T_{earth}, T_a, T_o, T_s are the physical temperature of the earth, atmosphere, object and space respectively and ε is the emissivity of the space object. The atmospheric absorption factor L_a is defined as

$$L_a = 10^{(L_{atm} R_a / 10^4)}$$

where L_{atm} is the atmospheric attenuation (dB/km) and R_a is the effective range through the atmosphere. Sample L_{atm} values are shown in Table 1. For cloud cover, R_a is the thickness through the clouds.

For most man made space objects the emissivity of the object in the MMW region is small. With the assumption of small ε, from Eq. (1) and Fig. 3 it can be shown that the effective temperature of the space object is dominated by the reflection from the warm earth. The effective background temperature as observed from the ground is dominated by the radiation coming directly from the cloud cover (for clear weather the effective background temperature as observed from the ground is dominated by radiation from space and is very low ~3 K). Table 2. lists some assumptions about the physical characteristics of the sources identified in Eq. (1) along with an estimate of the attenuation due to cloud cover, in this case about 0.5 km of clouds. With the assumptions made in Table 2, the contrast between the space object and the background is of order 200 K. The SNR depends on the contrast $\Delta T = T_{\text{received}} - T_{\text{background}}$ and the system noise (T_{noise}) and can be expressed as

$$SNR = 10 \log (\Delta T / T_{\text{noise}}) \tag{3}$$

where T_{noise} depends on the type of imaging technique used to form an image.

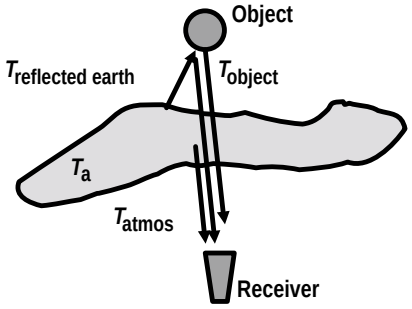

Fig. 3. Millimeter wave radiation received on the ground within the solid angle subtended by the object comes from T_{object} thermal emission from the object, $T_{reflected\ earth}$ – thermal emission from the atmosphere reflected off of the object, T_{atmos} thermal emission received directly from the atmosphere.

Table 2. Relative Parameters for Ground-Based MMW Imaging System. Effective Temperature Contrast Bewtween a Space-Based Object and the Background is ~200 k

Physical Temperature	Assumed Values (k)	Comments
T_{earth}	250	Temperature of earth
T_a	250	Temperature of clouds
T_o	100	Temperature of space object
T_s	3	Temperature of space
Emissivity of object (ε)	0.1	Metal object
Attenuation from atmosphere (L_a)	1.15	0.3 km cloud, 94 GHz
Effective temperature		
$T_{received} = T_{reflected\ earth} + T_{atmos} + T_{object}$	237	
$T_{rbackground} = T_{rspace} + T_{ratmos}$	35	
$T_{rreflected\ earth} = (1 - \varepsilon)\ T_{rearth}/L_a$	196	
$T_{ratmos} = T_{ra}\ (1 - 1/L_a)$	32	
$T_{robject} = \varepsilon T_{ro}/L_a$	9	
$T_{rspace} = T_{rs}/L_a$	3	
Effective temperature contrast	200	

4. IMAGING TECHNIQUES

There are many imaging methods that have been used to form MMW images. Fig. 4 illustrates three methods using real apertures (as opposed to a synthetic aperture), an optically focused imager [Fig. 4(a)], a sparse array [Fig. 4(b)], and a steerable sparse array [Fig. 4(c)]. The first two are commonly used imaging techniques, the third is a novel approach that addresses most of the issues that make the first two techniques difficult to apply to the AMOS mission needs.

Real Aperture

An optically focused imager uses either an optical lens or mirror to form a real image. An array of detectors need only detect the amplitude of the focused radiation to record a focused image. For this type of imager the system noise is $T_{noise} = T_{sys}/(B\tau)^{1/2}$, where T_{sys} is the noise of the receiver, B is the bandwidth of the receiver and τ is the integration time. For the parameters listed in Table 2, the SNR for an optically focused imager is larger 38. However because of the large aperture size required by the AMOS mission resolution requirements an optically focused system is obviously not practical.

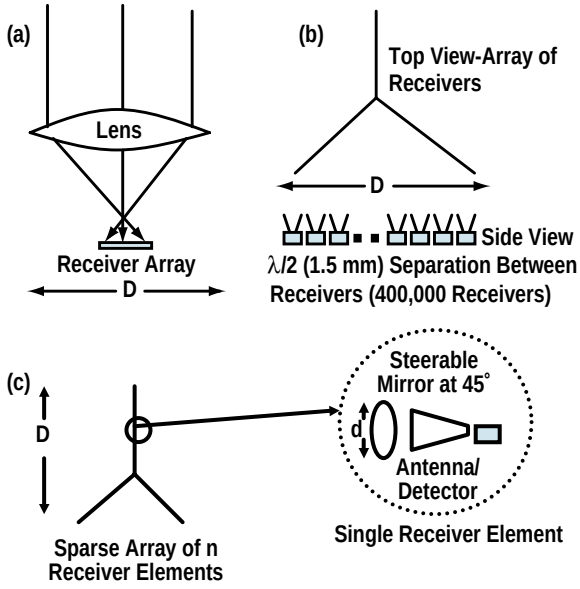

Fig. 4. Millimeter wave imaging system types (a) real aperture, lens or mirror, view from side; (b) sparse array, (c) steerable sparse array layout. View from above. D ~ 300 m, d ~ 10 cm, n ~ 1000.

Sparse Array

The sparse array shown conceptually in Fig. 4(b) uses an array of receivers that span the imaging aperture but do not fill the aperture. Typically the array is two-dimensional and does not have optically focusing elements in front of the receivers. (The receivers are said to be in the "pupil plane" [6,7,8].) To form an image the detectors must record both amplitude and phase of the incoming radiation wave front. The image is formed in the electronics (typically in software) by taking spatial Fourier transforms across the two axis of the array. The sparseness of the array refers to the fact that the receivers do not fill the entire aperture area, but are typically linear arrays formed as a cross or a "Y". A complete image can be formed as long as all of the spatial Fourier components are collected. The sparseness of the array reduces the amount of the collected radiation and reduces the SNR by the ratio of the area of the receivers to the area of the complete aperture. The reduction in SNR is shown in Table 3.

Table 3. Comparison Between Imaging Techniques. 300 m Diameter Imagers, 200 km Range, Clouds or Light Rain, Individual Receiver Noise ~ 1000 k. Bandwidth (B) 1 GHz, Integration Time of 1 s.

Imaging Technique	No. of Receivers	T_{noise} (k)	SNR
Real aperture	10,000	0.03	38
Sparse array	400,000	33	8

In a conventional sparse array the field of view (FOV) is fixed and large to avoid having to physically steer the entire array to view different objects of interest. The FOV of the array is determined by the antenna pattern of the individual receivers in the array. (See Fig. 5 for the geometry for this discussion.) The FOV of the main lobe of the antenna pattern for an individual receiver is approximately Eq. (4) $\theta \sim \lambda/d$. To observe most of the sky requires that the individual receiver size be ~λ/2. This large FOV places restrictions on the density of receivers in the linear arrays that form the sparse array. Phase ambiguities occur at view angles (θ) that satisfy Eq. (5) $v \sin(\theta) = n \lambda$, where v is the space between receivers, n is a positive integer. (These ambiguities are called grating lobes.) To avoid the grating lobe ambiguity, the FOV should be smaller than the separation between the grating lobes or $d > v/2$. This implies that to view most of the sky requires detector spacing of approximately λ. To satisfy the AMOS mission requires an impractical number of receivers using the conventional sparse array method. This is shown graphically in Fig. 6 where the large numbers of receivers come both from SNR requirements and the receivers spacing requirements to avoid the grating lobes.

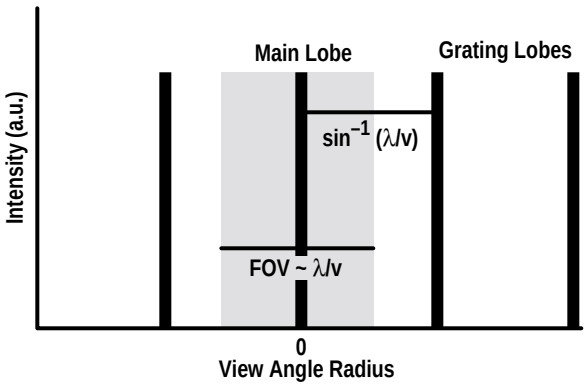

Fig. 5. Antenna pattern for a sparse array. *v* is the spacing between receivers, *d* is the individual receiver size. To avoid the grating lobe ambiguity the FOV of the array should be narrower then the closest grating lobe. This leads to a the relation between the receiver spacing and the receiver size $d>v/2$.

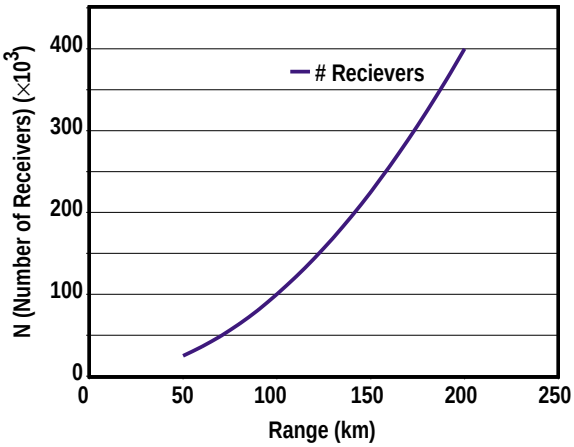

Fig. 6. Number of detectors required for a conventional sparse array vs. range. Fixed resolution of 2 m, SNR of 8, 0.5 km of cloud cover. Other parameters as shown in Tables 1 and 2.

Steerable Sparse Array

To address the problem of requiring a large number of receivers while maintaining the resolution, SNR and FOV requirements we propose a sparse array of receivers with each receiver have a steerable mirror. The geometry is shown in Fig. 4(c). The steerable mirrors allow the receivers to have large individual antennas with a narrower FOV. Tracking or searching of objects would be accomplished by steering the mirrors. The large individual antennas allow a dramatic reduction in the number of receivers while maintaining good overall performance of the array. The performance of a steerable array is expressed as follows

$$T_{\text{noise}} = T_{\text{sys}}\, D^2\, \theta^{3/2}\, (B\tau)^{-1/2}/NR\lambda^2 \tag{4}$$

The large area antennas increases the detected signal in each receiver by the area of the antenna and allow larger spacing between the receivers while avoiding the grating lobes [Eq. (5)]. Fig. 7. is a plot of the number of receivers versus the array FOV. The mirrors allow the FOV of the array to be moved to cover most of the sky, however very large individual mirror/receiver assemblies are probably undesirable as is a very narrow FOV.

5. STEERING OPTIONS

Steering the individual antennas can be accomplished by mechanical mirrors, moving the receiver antennas or by an electronically steerable mirror. The attitude of the receiver antenna pattern must be known to roughly resolution/range in radians (~5 microradians for 200 km and 1 meter resolution). This requirement can be reduced somewhat by using autofocus algorithms but in general high pointing accuracy is required. The mechanical pointing techniques are well established and low risk but from a system standpoint are costly because of the large number of detectors required. Electronically steered mirrors refer to devices in front of the receivers that can introduce large controllable, optical phase delays. There are several possible electronically steerable mirror concepts including soft ferrite modulators and patched phased arrays [9,10]. We focus here on a single promising solid state technology. A flat mirror constructed from a metal mirror with a GaAs wafer over the mirror with a metal strip grid introduces an phase shift in the reflected radiation dependent on the impedance of the metal strip array (Fig. 7). The impedance is determined by the inductance due to the metal strip and the capacitance from the gap between the strips. By loading the metal grid with bias able varactor diodes, the capacitance between the metal strips can be controlled. This allows direct control of the impedance at each gap site and thus direct control of the phase delay of the reflected radiation. The diodes can be made monolithically within the GaAs with the metal strips serving as controllable bias lines. Very fast steering of the beam is possible. This type of steerable mirror has the potential of being low cost and very flexible.

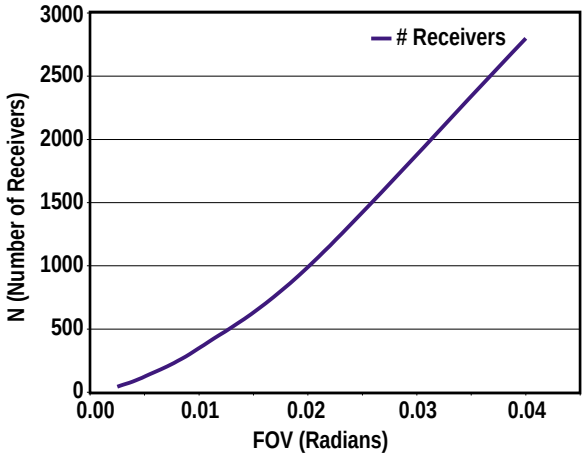

Fig. 7. Number of receivers required vs. instantaneous FOV for a steered sparse array with a fixed SNR of 14, range 200 km, with resolution of 2 m.

6. POINT DESIGN

To give some idea of what a AMOS MMW imaging system might look like we present here a conceptual point design. The array would be spread across the Haleakala site in a rough Y shape following the general landscape. While most sparse arrays are two-dimensional, variations in placement can be tolerated. Large vertical variations (displacement of the receivers in the direction of the range) can be tolerated by including the appropriate phase delay in the receiver electronics to compensate for the time delay due to the longer (or shorter) range. Holes in the linear arrays making up the arms of the array can also be tolerated as long as the number of receivers is maintained (SNR) and most of the Fourier spatial components are retained. Detailed modeling of the antenna pattern and resultant resolution would be required to optimize the placement of the receivers within the physical constraints of the site. The individual antenna diameters would be of order 10 cm giving a FOV of approximately 10 km at 200 km attitude. The total number of receivers required would be 1000. This system would be able to image space objects at 200 km altitude with roughly 1 meter resolution and SNR and contrast greater then five with 0.5 km of cloud cover.

7. ARRAY CALIBRATIONS AND OTHER ISSUES

Receiver Position Measurement

The image formation of the of a sparse array relies on an accurate measure of the radiation wave front including relative phase. To reconstruct the wave front from which the image in then formed requires accurate receiver location knowledge. For good image quality phase resolution better then 60 degrees is required. This then requires that the relative location knowledge of the receivers must be better then l/6 ~ 500 microns. While initial receiver position can be determined by careful surveying vibrations and thermal swelling of the support structures and the ground will move the positions of the receivers by more then 500 microns. A real time motion measurement system is needed to track the motion of all of the receivers. For a small number of receivers inertial measurement units (IMU) using accelerometers and gyroscopes would be possible but cost prohibitive for the large number of receivers in the proposed array. A possible low cost solution is to use elevated coherent MMW beacons that would be visible from all of the receivers. A narrow band signal from the beacons would be used to measure motion relative to the beacons by measuring phase shifts in the narrow band signal at each of the receivers. A minimum of three beacons would be required to track the motion in all three axis. This technique uses the receivers and associated electronics to measure the motion without additional hardware at each of the receivers. The beacons would not in general be in view of the FOV on the receivers but even with very low beacon power there should be sufficient coupling to the receivers through the side lobes. The beacons also potentially solve another calibration issue, namely phase errors due to drifts in the electronics, cable length changes due to thermal drifts and other phase errors. Calibration of the phase shifts not associated with motion of the receiver would require a fourth beacon.

The relative gain of the receivers, required for image formation, can be measured using the signals from the MMW beacons. The coupling efficiency of the beacon signal into the receiver through the side lobes will be very sensitive to the position of the steerable mirror. To calibrate the gain of the receivers the mirrors will have to be positioned at some known angle during the calibration. Typically the gain of the receivers drifts on a time scale long compared to the image formation time. This would allow the gain calibration to be done on a periodic schedule with minimal disruption to the imaging system.

Algorithm and Processing Requirements

The number of operations required to form an image goes roughly as the number of receivers squared. Further, the motion measurements and phase calibrations will require significant real time processing requirements but only scale as the number of detectors. It is anticipated that the AMOS supercomputer center will be able to provide the required processing.

The long integration time (~1 s) required to give an acceptable SNR presents an image formation challenge. The high velocities of the space objects will cause large smearing in the image. Algorithms to focus the image will have to be developed. Fortunately space objects mostly move in smooth trajectories, and this can be exploited in the focusing algorithms.

8. SUMMARY

Passive MMW imaging has the potential for allowing operation of the AMOS sensor in poor weather, improving its capability to fulfill its mission in tracking and identify space objects. Due to the long wavelength, MMW imaging systems capable of contributing to the AMOS mission are inherently large. We have presented a novel concept for a MMW imaging system that, while the aperture is still large, the overall system is of manageable size and complexity. A sparse array with steerable mirrors allows the imager to operate with good SNR, large effective FOV with a relatively small number of receivers. The system would provide resolution. We have identified a number of challenging calibration and related issues with concepts for addressing them. The most critical calibration is measuring the relative position of the receivers.

9. ACKNOWLEDGEMENT

Work supported in part under U.S. Department of Energy Grant DE-FG03-01ER54615. The authors would like to thank Will Otaguro for his contributions to this work.

10. REFERENCES

1. Medrano Tsgt , R., "Overview of the Maui Space Surveillance System," 2001 AMOS Technical Conference, Kihei, HI, 2001.
2. Peng, Q., Snider, R.T., Cowan, T.E., Herman, S.M., Perry, M.D., Schissel, D.P., "LIDAR Cloud Penetration Simulator," 2001 AMOS Technical Conference, Kihei, HI, 2001.
3. Smith, E.K., "Centimeter and Millimeter-Wave Attenuation and Brightness Temperature Due to Atmospheric Oxygen and Water Vapor," *Radio Science* **17**, p. 1445, 1982.
4. Silverstein, J.D., "Passive Millimeter-wave Image Resolution Improvement by Linear and Nonlinear Algorithms," in *Passive Millimeter-wave Imaging Technology II*, R.M. Smith, ed., Proc. SPIE 4373, p. 132, 2001.
5. Gleed, D.G., Lettington, A.H., and Hong, Q.H., "Comparison of Methods for Super-Resolving Passive Millimeter-Wave Images," in *Applications of Digital Image Processing XIX*, A.G. Tescher ed., Proc SPIE 2847, p 292, 1996.
6. LeVine D.M., Swift, C.T., Haken, M., "Development of the Synthetic Aperature Microwave Radiometer, ESTAR," I*EEE Transactions on Geoscience and Remote Sensing* **39**, p. 1999, 2001.
7. Edelson, C., "SyntheticArray Radiometry," Proc. IGARSS, p. 1429, 1992.
8. Milman, A.S., "A Cross Antenna for Passive Microwave Remote Sensing," Proc. IGARSS, p. 1423, 1987.
9. Seeds, A.J., DeSalles, A.A., "Optical Control of Microwave Semiconductor Devices," *IEEE Trans MTT* **38**, p. 577, 1990
10. Dou, W.B., Zeng, G., Sun, Z.L., "Quasi-Optical Ferrite Switches Ued in Radiometric," *Int. J. IR and Millimeter-Waves* **17**, p. 1193, 1996.